MDPI

Article

Pyrrolidinium-Based Ionic Liquids as Advanced Non-Aqueous Electrolytes for Safer Next Generation Lithium Batteries

Antía Santiago-Alonso [1,2], José Manuel Sánchez-Pico [1], Raquel San Emeterio [1], María Villanueva [1], Josefa Salgado [1,*] and Juan José Parajó [1,*]

1 NaFoMAT Research Group, Physic Faculty and Materials Institute (iMATUS), Universidade de Santiago de Compostela, Rúa de José María Suárez Núñez, s/n, 15782 Santiago de Compostela, A Coruña, Spain; antia.santiago.alonso@usc.es (A.S.-A.); josemanuel.sanchez.pico@rai.usc.es (J.M.S.-P.); raquel.san@rai.usc.es (R.S.E.); maria.villanueva@usc.es (M.V.)
2 ABCR LABORATORIOS, Lg. Vilapouca (PG Industrial), 36550 Forcarei, Pontevedra, Spain
* Correspondence: j.salgado.carballo@usc.es (J.S.); juanjose.parajo@usc.es (J.J.P.)

Abstract: In the current context of increasing energy demand, ionic liquids (ILs) are presented as possible candidates to replace conventional electrolytes and to develop more efficient energy storage devices. The IL 1-Methyl-1-propylpyrrolidinium bis(trifluoromethanesulfonyl)imide has been selected for this work, due to the good thermal and chemical stabilities and good electrochemical performance of the pyrrolidinium cation based ILs. Binary mixtures of this IL and lithium salt with the same anion, [TFSI], have been prepared with the aim of assessing them, as possible electrolytes for lithium batteries. These mixtures were thermally and electrochemically characterised through DSC and dielectric spectroscopy studies. The ionic conductivity decreases as the salt concentration increases, finding values ranging between 0.4 S/m and 0.1 S/m at room temperature. Additionally, a wide liquid range was found for the mixtures, which would reduce or even eliminate some of the most common problems of current electrolytes, such as their crystallisation at low temperatures and flammability. Finally, the toxicity of pure IL and the intermediate salt concentration was also evaluated in terms of the bioluminescence inhibition of the Alivibrio Fischeri bacteria, observing that, although the toxicity increases with the salt addition, both samples can be classified as practically harmless.

Keywords: ionic liquids; battery safety; non-aqueous electrolyte; DSC; BBDS; Microtox®

1. Introduction

One of the biggest challenges for contemporary society is the transition to a new energy model based on renewable resources instead of fossil fuels. This transition involves many demanding tasks that must be taken up by science and the whole society, including sustainable consumption, material recycling, and the circular economy. An-other fundamental aspect that needs to be addressed is the primary issue posed by renewable sources: their intermittency. Their output depends on environmental factors, seasonal variations, weather conditions, and the day/night cycles. As a result, peak production frequently does not coincide with peak demand, underscoring the necessity for systems to store surplus energy. For this reason, the development and innovation of energy storage systems is currently a strategic line. The actual battery market is dominated by lithium-ion batteries (LIBs) due to their numerous advantages over other battery systems. These include high specific capacity and voltage, a wide operation temperature range, excellent cycling performance, minimal self-discharge, and the absence of memory effects [1].

Nowadays, most LIBs are composed of a carbonate(s) in combination with a lithium salt [2]. Nevertheless, common carbonates have a flash point near room temperature, making them highly inflammable if exposed to extreme thermal, electrical, or mechanical conditions, in which can lead to serious events such as fire or explosion [3]. While the risk

of failure in a single cell is minimal, the risk increases significantly when thousands of cells are enclosed in a single battery pack.

Aqueous-based electrolytes present advantages over carbonate-based ones in terms of safety and cost. Nevertheless, they exhibit lower energy densities, narrower electrochemical stability windows, and limitations at temperatures below the crystallisation point of water [4].

Ionic liquids (ILs) have recently attracted considerable interest because of their exceptional properties and potential applications across diverse fields. The ILs are composed entirely of ions and exist in the liquid state at temperatures below 100 °C. The identifying characteristic of ILs is their low volatility, which makes them environmentally friendly alternatives, reducing the risk of air pollution and flammability [5,6]. One of the most intriguing aspects of ILs is their tunability. By selecting different combinations of cations and anions, it is possible to customize their physical and chemical properties to match a particular application. This adaptability extends to their thermal and electrochemical stability, solubility, viscosity, and ionic conductivity [4]. For instance, ILs can be designed to dissolve a large sort of substances, including organic, inorganic, and polymeric substances, making them highly effective solvents for chemical reactions and extractions [7].

Moreover, ILs have unique solvation properties with significant implications for green chemistry, where ILs are used to replace volatile organic solvents, minimizing the environmental impact [7]. So, to overcome the problem of common carbonates, ionic liquids (ILs) and their blends with electrochemically relevant salts emerge as a viable alternative. These mixtures offer enhanced safety, non-flammability [8] and thermal stability, without compromising electrochemical performance [9].

The effectiveness of ionic liquid–Li-ion electrolyte solutions is directly influenced by Li-ion mobility, which is intricately linked to their local environment, including solubility and solvation properties, [7,10].

Between the practically unlimited combinations of ILs, pyrrolidinium based ILs emerge as a clear alternative due to their exceptional thermal and electrochemical stability, versatility, and compatibility with Li-based battery materials [11,12]. N-methyl-N-propylpyrrolidinium bis(trifluoromethanesulfonyl)imide ($[C_3C_1Pyrr][TFSI]$) was selected due to the favourable characteristics of pyrrolidini-um-based ionic liquids [13]. Since ILs are not inherently electroactive, their use in LiBs requires mixing with lithium salts. Instead of the frequently used $LiPF_6$ for the electrolytes preparation, lithium bis(trifluoromethanesulfonyl) imide (LiTFSI) was selected, whose high conductivity, resistance to moisture, and extraordinary thermal and electrochemical stability makes it a good alternative to the $LiPF_6$ salt [14].

The aim of this study is to advance the properties knowledge of ILs and their mixtures and their subsequent potential use in energy storage systems. Therefore, we propose a comprehensive analysis of the thermal behaviour, electrical conductivity, and ecotoxicity of mixtures of N-methyl-N-propylpyrrolidinium bis(trifluoromethanesulfonyl) imide ($[C_3C_1Pyrr][TFSI]$) and lithium bis(trifluoromethanesulfonyl)imide ($[Li][TFSI]$) at different concentrations.

2. Materials and Methods

2.1. Chemicals

The IL, 1-Methyl-1-propylpyrrolidinium bis(trifluoromethylsulfonyl)imide ($[C_3C_1Pyrr][TFSI]$) provided by IoLiTec, was selected for this work due to its promising electrochemical properties as it is reported by different authors [15–17] and, as is also mentioned before, their non-flammable character. The salt lithium bis(trifluoromethylsulfonyl)imide ($[Li][TFSI]$) was provided by Sigma Aldrich, sharing the anion with the IL. Table 1 summarizes the key characteristics of the ionic liquid and the salt, being the stated purity of both higher than 0.99. To know the effect of salt concentrations on the physicochemical and biological properties, mixtures of four different concentrations (mole of salt per litre) ranging from 0.2 m to 1 m were analysed (Table 2).
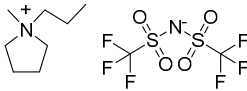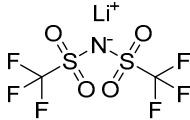
Table 1. Reagent used in this study.

Name	Molecular Mass (g·mol^{-1})	Structure	Short Name CAS Number
1-Methyl-1-propylpyrrolidinium bis(trifluoromethylsulfonyl)imide	408.38		[C$_3$C$_1$Pyrr][TFSI] 223437-05-6
Lithium bis(trifluoromethylsulfonyl)imide	287.09		[Li][TFSI] 90076-65-6

Table 2. Amount of pure metal salts per kilogram of [C$_3$C$_1$Pyrr][TFSI] in the mixtures.

Molality/mol kg^{-1}	m$_{LiTFSI}$/g
0.2	57.42
0.5	143.55
0.75	215.32
1.0	287.10

2.2. Differential Scanning Calorimetry

The thermal behaviour and thermal transitions of the mixtures IL + salt were analysed using the Differential Scanning Calorimeter DSC Q2000 (Waters-TA Instruments. New Castle, DE, USA) with hermetically sealed aluminium pans, samples mass of (5–8) mg and nitrogen atmosphere. For the experimental part two heating-cooling cycles between −80 °C and 100 °C at two different rates, 10 °C min^{-1} and 5 °C min^{-1}, have been carried out, after an initial ramp from room temperature to 125 °C at 40 °C min^{-1} with an iso-thermal step at 125 °C for 45 min, to remove possible volatile impurities. Transition temperatures were determined as the onset point of the different peaks from the DSC curves during the reheating and re-cooling ramps. Transition temperatures were estimated with an uncertainty of 2 °C at 95% confidence [18]. Further details can be found in previously published papers [19,20].

2.3. Ionic Conductivity

Ionic conductivities were measured through broadband dielectric spectroscopy using an Agilent RLC precision meter HP 4284A (Agilent Technologies, Santa Clara, CA, USA) with a precision of 0.05% in the measurements. The applied frequency range was 20 Hz to 0.2 MHz to ensure a good fitting of the ohmic regime with a tolerance for the slope of the imaginary part of the dielectric constant of −1.00 ± 0.02 described thoroughly by J. Leys [21]. The mixtures were analysed using a symmetric two-electrode Swagelok configuration with stainless-steel electrodes, this setup ensures that the distance between electrodes remains constant. To control the temperature, the Swagelok cell was placed in a climate chamber (Memmert ICP400, Schwabahc, Germany); measurements were pursued in the range of 0 °C to 50 °C, starting with the lowest temperature. The experiment was done following a static isothermal method with an extra 15 min to assure the thermal equilibrium inside the chamber before performing the measurement.

2.4. Toxicity

The toxicity of the pure [C$_3$C$_1$Pyrr][TFSI] and the mixture of intermediate concentration (0.5 m) with [Li][TFSI], selected based on melting and conductivity results, was assessed using the Microtox® Toxicity Test kit (M500 Analyzer—Modern Water, Rema Tek LLC, Bonsall, CA, USA), following the procedure detailed in previous studies [22,23]. The Microtox® test measures the luminescence inhibition in the Gram-negative marine

bacterium *Aliivibrio fischeri* (*A. fischeri*) by targeting a quorum sensing mechanism. When exposed to a toxic substance, bacterial respiration is disrupted, leading to a de-crease in bioluminescence, which correlates directly with the metabolic activity of the bacterial population. The results were compared with previous data on ILs of the same and different nature.

A range of diluted aqueous solutions (0 to 81.9%) of each compound was prepared for the acute toxicity test, with exposure times of 5, 15, and 30 min. The resulting data were used to estimate the effective concentrations causing 50%, 20%, and 10% (EC_{50}, EC_{20}, and EC_{10}, respectively) luminescence inhibition. The 95% confidence intervals were also calculated using non-linear regression and the least-squares method to fit the data to the logistic equation [22,23].

Passino and Smith [24] proposed six toxicity levels in their widely used toxicity classi-fication based on EC50 values at 30 min, as follows: $EC_{50} > 1000$ mg/L: relatively harmless; 1000 mg/L > EC_{50} > 100 mg/L: practically harmless; 100 mg/L > EC_{50} > 1 mg/L: toxic; 1 mg/L > EC_{50} > 0.1 mg/L: highly toxic; 0.1 mg/L > EC_{50} > 0.01 mg/L: extremely toxic and EC_{50} < 0.01 mg/L: super toxic.

3. Results

3.1. DSC Results

The comparison of DSC curves registered on cooling and on subsequent heating at 5 C min^{-1} for mixtures of [C$_3$C$_1$Pyrr][TFSI] + [Li][TFSI] and pure IL, are presented in Figure 1. As it can be observed, pure IL shows a unique peak on both, cooling and heating scans, which correspond to freezing and melting processes, respectively. The shift between the onset temperatures of these two peaks, around 20 °C; known as the super-cooling effect, is common in ILs due to the difficulty of crystallization that these com-pounds present where in addition to the Coulomb forces, Van der Waals interactions have great importance [20,25].
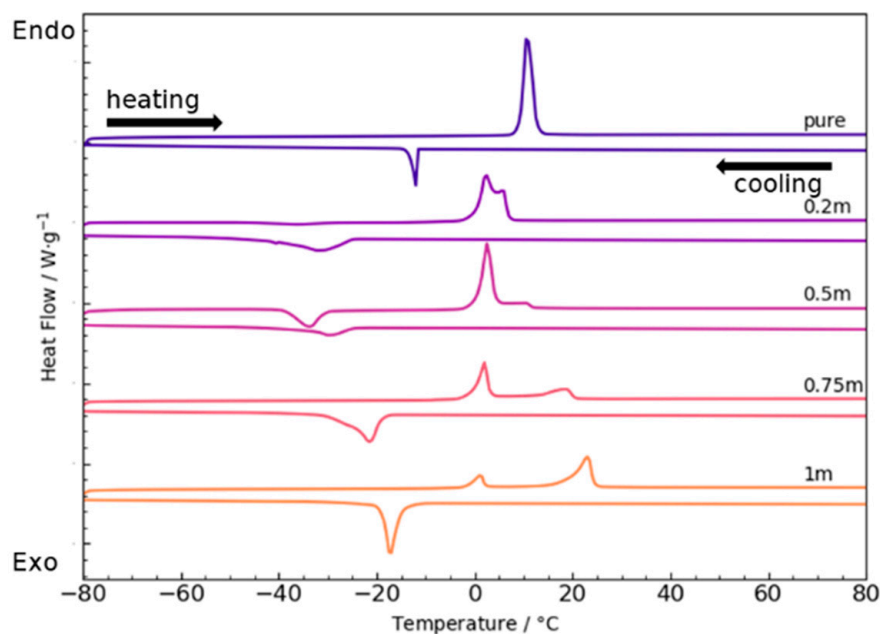

Figure 1. DSC curves of binary mixtures [C$_3$C$_1$Pyrr][TFSI] with [Li][TFSI] at different concentrations (endo up).

Table 3 summarizes the values of the characteristic temperatures and enthalpies, determined as the onset temperature and area of the corresponding peak respectively. Onset temperatures corresponding to the melting and freezing of the pure IL are in good con-cordance with findings reported by other researchers [26–33].

Table 3. Temperature of glass transition (t_g), melting (t_f), freezing (t_c), and cold crystallisation (t_{cc}) and freezing, melting, and cold crystallisation enthalpies obtained from DSC curves.

Sample	$t_g/°C$	$t_f/°C$	$t_{m,1}/°C$	$t_{m,2}/°C$	$t_{cc}/°C$	$\Delta_{cc}H$ /J g^{-1}	$\Delta_f H$ /J g^{-1}	$\Delta_f H$ /kJ mol^{-1}	$\Delta_m H$ /J g^{-1}	$\Delta_m H$ /kJ mol^{-1}
[C$_3$C$_1$Pyrr][TFSI]	--	−12	9	--	--	--	−33	−13	36	15
0.2 m	--	−25	0.3	6	−46	−2.6	−22	−10	34	15
0.5 m	−74	−25	0.7	10	−39	−13.9	−10	−5	34	16
0.75 m	−69	−19	−0.1	19	--	--	−24	−12	27	13
1.0 m	--	−15	−1.4	19	--	--	−24	−13	23	12

The thermal behaviour of IL + salt mixtures reflects important differences compared to the pure IL, and they are highly dependent on both the molar fraction of the [Li][TFSI] salt and the scanning rate, as shown in Figures 2 and 3. Thus, DSC curves upon heating corresponding to the 10 °C min^{-1} (blue) and 5 °C min^{-1} (red), presented in Figure 2, show that the scanning rate does not influence the thermal behaviour of pure IL, as the onset and peak area of the melting peak are similar for both experiments, although this is not fulfilled for the mixtures with the lithium salt. As observed, the cycle at 10 °C min^{-1} presents an exothermic cold crystallization peak upon heating for mixtures of 0.2, 0.5 and 0.75 m of [Li][TFSI] samples; but these peaks became smaller or even disappeared after recooling and reheating the sample at 5 °C min^{-1}. In all cases, the onset of cold crystallization as well as the area of the corresponding peak change with the scanning rate. This is due to the fact that this event is a kinetically controlled process, and crystallization is challenging at high scanning rates, even though it is the most stable form; which subsequently causes additional crystallization of the sample upon heating. However, at lower rates, the sample completely crystallizes during the cooling ramp, and therefore the exothermic peak upon heating, the cold crystallization process, disappears. This can be seen in Figure 3, in which the cooling-heating cycles of the mixture of IL + [Li][TFSI] 1 m at 10 °C min^{-1} and 5 °C min^{-1} are presented, and the reduction of the cold crystallization peak with decreasing scanning rate is clearly visible. It is important to highlight that the melting process is a thermodynamically controlled transition, and the onset of the corresponding peak does not depend on the scanning rate.

Another notable observation is the splitting of the initial melting peak into two distinct peaks of different sizes as salt is introduced into the mixture, even though the molar heats associated with the overall process remains similar to those corresponding to the pure IL, as shown in Table 3. With increasing molar fraction of lithium salt, the resolution of both peaks increases, and the second peak even becomes the most intense at the highest salt concentration. This suggests the coexistence of two different polymorphic states, which is in good concordance with the findings of Hendersson and Passerini [29] for these mixtures and recent results from our group with different mixtures of IL + inorganic salt [34,35]. By increasing the salt concentration in the mixture, the crystallinity tends to decrease, that means an increase of amorphous behaviour, reflected by the disappearance and reduction of crystallization and fusion peaks and the appearance of glass transitions at higher temperatures. For pure IL and lower molar fractions, no glass transitions were detected within the experimental temperature range (T > −80 °C). Although, in our case, crystallization and melting peaks appear for all the mixtures, a clear loss of peak definition with higher salt concentration is observed, connected to the increase of amorphous behaviour with salt addition.
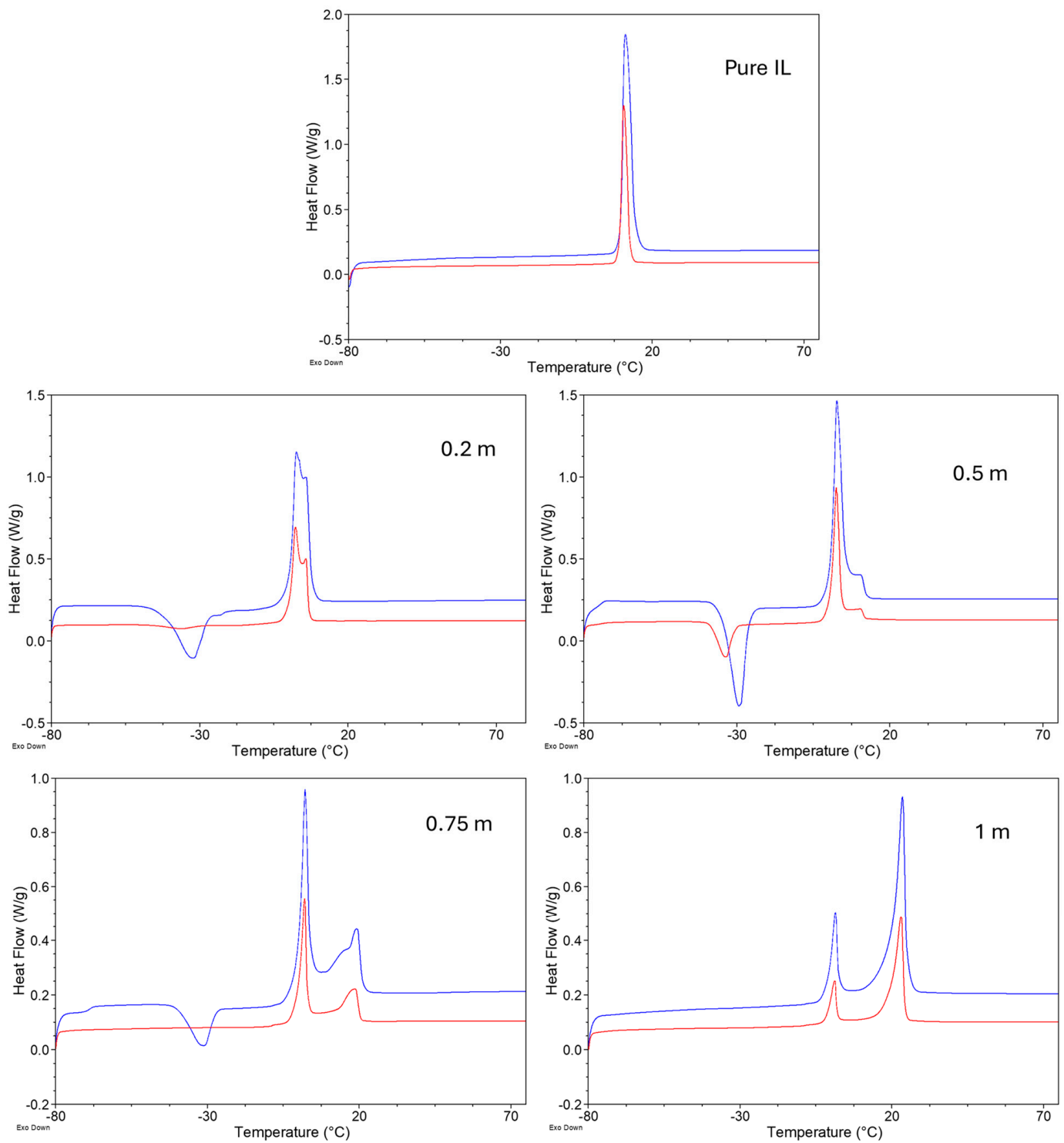
Figure 2. First (blue) and second (red) heating curves corresponding to 10 °C min^{-1} and 5 °C min^{-1} scan rates, respectively, for the pure and mixtures of IL + salt samples (endo up).
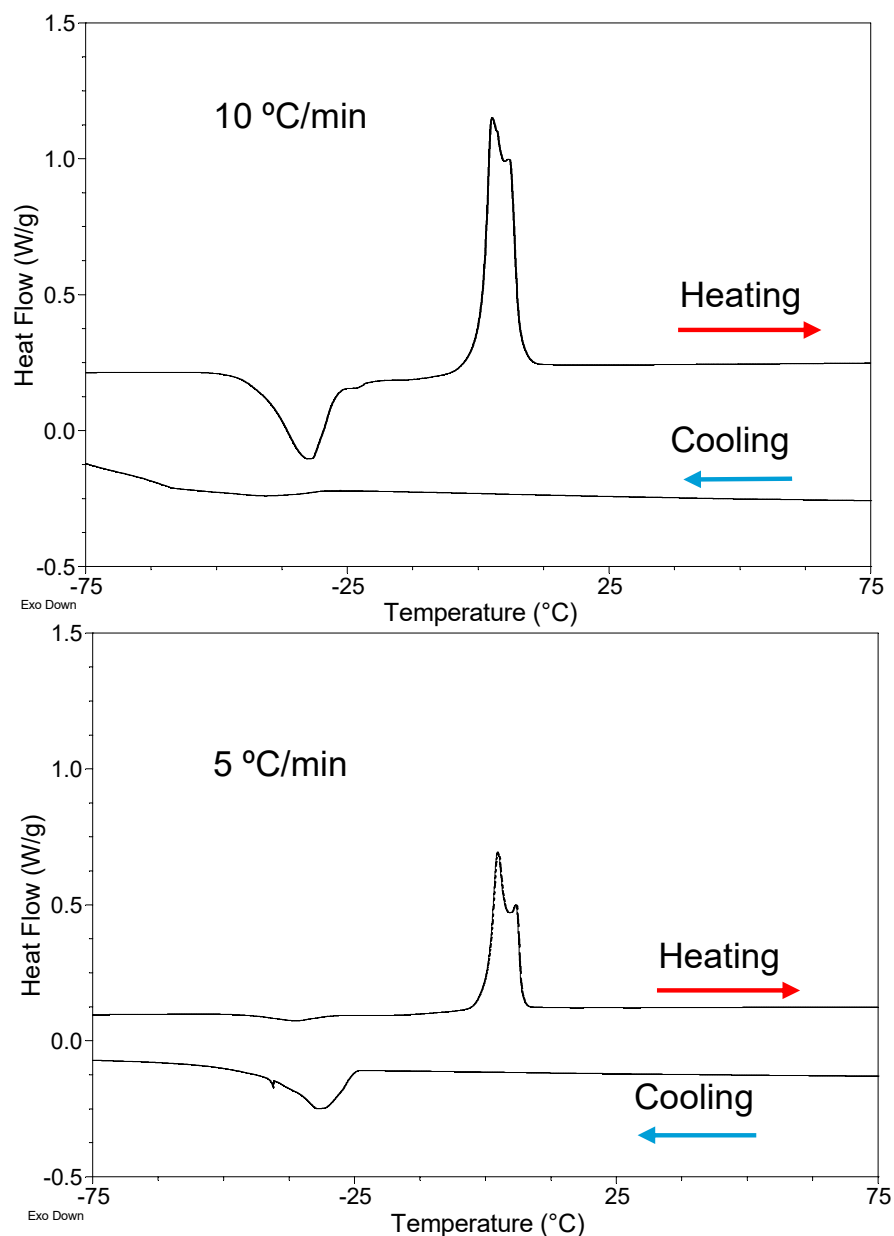
Figure 3. DSC cooling-heating cycles at 10 °C min^{-1} and 5 °C min^{-1} of the mixture IL + [Li][TFSI] 0.2 m (endo up).

3.2. Ionic Conductivity Results

Dielectric measurements were carried out from high to low temperatures to use the supercooling effect of these samples, as previously pointed out. The ionic conductivity of binary mixtures of [C$_3$C$_1$Pyrr][TFSI] and [Li][TFSI] are shown in Figure 4a against molality of [Li][TFSI] and Figure 4b against temperature in Arrhenius representation. The ionic conductivity for pure [C$_3$C$_1$Pyrr][TFSI] agrees with previously published results [15–17,26]. Regarding [C$_3$C$_1$Pyrr][TFSI] + [Li][TFSI] mixtures, their ionic conductivity follows the expected pattern, a decrease with higher molalities of salt [36], reaching 0.1180 S/m at 298 K at the highest molal concentration. This decrease is related with the increment of the viscosity. However, other authors pointed that the formation of diffusing [Li(TFSI)$_n$]$^{-(n-1)}$ ionic species in the solutions might lead to a decrease in conductivity [17,28]. Table 4 shows the ionic conductivities of all mixtures.
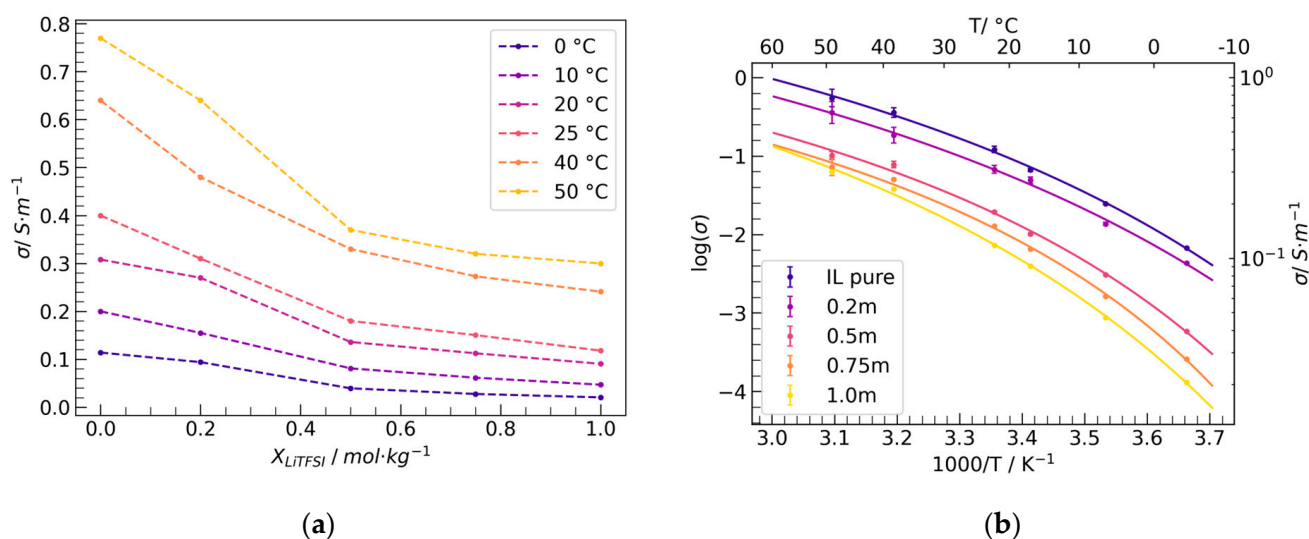
Figure 4. (**a**) Ionic conductivity of binary mixtures [C$_3$C$_1$Pyrr][TFSI] and [Li][TFSI] against the [Li][TFSI] molar fraction at different temperatures. (**b**) Arrhenius plot showing the ionic conductivity vs. temperature for mixtures with different [Li][TFSI] content and their fitting to the Arrhenius equation.

Table 4. Ionic conductivities (in S.m^{-1}) of pure IL and IL + [Li][TFSI] salt for different concentrations and temperatures.

Temperature/°C	IL Pure	0.2 m	0.5 m	0.75 m	1.0 m
0	0.1138(37)	0.0936(71)	0.0394(15)	0.02764(17)	0.020539(95)
10	0.200(11)	0.155(20)	0.0810(50)	0.06148(62)	0.04694(32)
20	0.308(21)	0.267(41)	0.1364(99)	0.1125(19)	0.0905(10)
25	0.397(38)	0.305(48)	0.180(15)	0.1504(30)	0.1180(16)
40	0.645(59)	0.48(10)	0.325(40)	0.2726(89)	0.2412(57)
50	0.77(11)	0.64(14)	0.373(49)	0.32(11)	0.2998(79)

The ionic conductivity behaviour against temperature (shown in Figure 4b) is widely described in the literature by the Vogel-Fulcher-Tammann (VFT) equation (Equation (1)). At low temperatures the relaxation and transport properties become slower due to the glass transitions that these ILs typically present [37] giving a non-monotonic behaviour against temperature, described by this VFT-equation:

$$\log \sigma = \log \sigma_\infty - \frac{B}{(T - T_0)} \tag{1}$$

In the VFT equation, σ_∞ represents the ionic conductivity at infinite temperature, B is the fragility index or strength index, which inversely correlates with liquid's kinetic fragility, and T_0, also known as Vogel temperature, is the temperature at which mobility vanishes. The VFT parameters obtained from the individual fitting of the samples are compiled in Table 5. The conductivity at infinite temperature shows small variations with salt concentration, as previously reported [35]. A similar behaviour is observed for B and T_0.

Although VFT model fits to experimental data, the resulting dependence on salt concentration shows behaviours that are challenging to explain physically. None of the fitted parameters represent a clear relation with salt concentration, as also observed by Tsamopoulos & Wang [38]. In their work, they demonstrated that the fitted values of T_0 fails to follow the variations in glass transition temperature with salt concentration, and likewise, unphysical fluctuations in σ_∞ and B are found.

Table 5. Fitting parameters of VFT and Arrhenius equations for all samples.

Sample	VFT-Equation			Arrhenius Equation		
	Log σ_∞	B/K^{-1}	T_0/K	log (σ_∞)	E_a (10^{-1})/eV	R^2
IL pure	2.49(54)	326(98)	203(13)	10.36(71)	2.93(18)	0.98
0.2 m	2.38(72)	351(95)	199(21)	10.01(69)	2.89(17)	0.98
0.5 m	1.66(69)	274(87)	217(11)	11.6(11)	3.46(28)	0.97
0.75 m	1.40(47)	246(64)	223.3(86)	12.5(12)	3.75(33)	0.96
1.0 m	2.19(54)	372(89)	211.8(94)	13.7(11)	4.10(29)	0.98

In the case where $T \gg T_0$, a linear behaviour in the Arrhenius plot can be obtained, and the approximation of the VFT equation by the Arrhenius equation is valid.

$$\log \sigma = \log \sigma_\infty - \frac{E_a}{k_{\mathrm{B}} T} \tag{2}$$

where E_a represents the activation energy per molecule and k_{B} the Boltzmann constant.

The fittings for all the samples to the Arrhenius equation were calculated and presented in Table 5 and represented in Figure 5a.
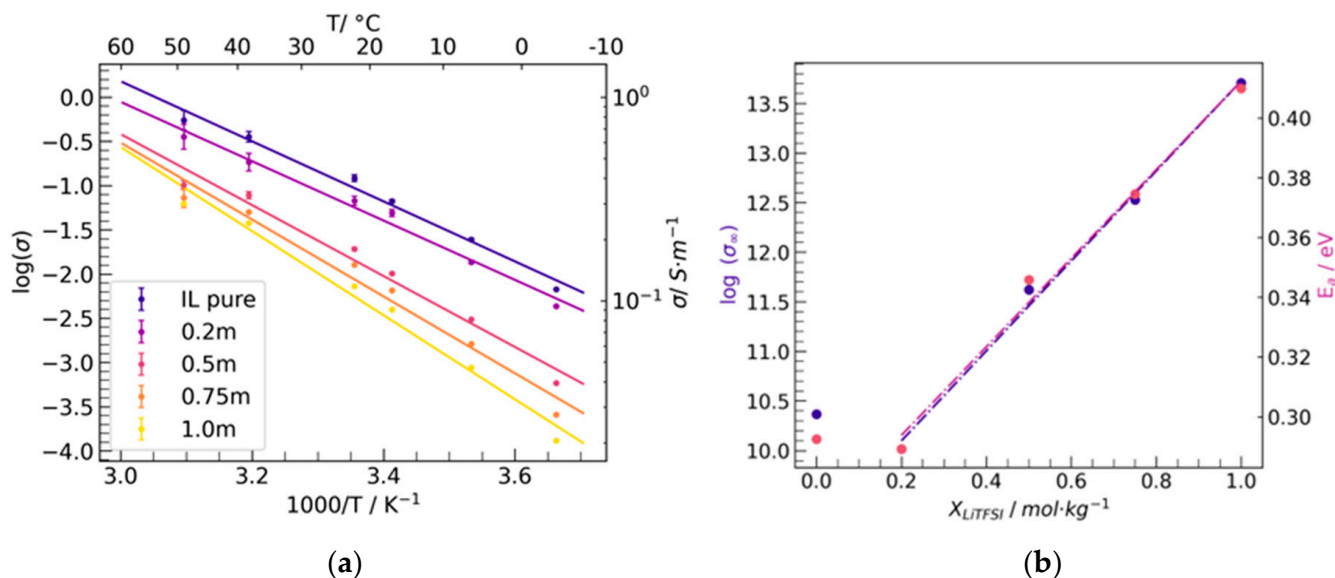

(a) **(b)**

Figure 5. (**a**) Arrhenius plot of the ionic conductivity vs. temperature for mixtures with different [Li][TFSI] contents and their fitting to the VFT equation, and (**b**) activation energy and log (sigma) dependence on the molal concentration of lithium salt.

Regarding the physical meaning of the fitted parameters, it is clear that both activation energy and $\log \sigma_\infty$ follow an increasing monotonic behaviour with salt concentration for all IL and salt mixtures, as shown in Figure 5b. The monotonic increase with salt concentration of the exponential factor in the Arrhenius equation is related to the increase in the dielectric constant [39]. The linear increase in activation energies with salt concentration indicates that ion conduction in the electrolyte requires more energy to take place, which is consistent with the decrease in ionic conductivity.

3.3. Toxicity Evaluation

Figure 6 shows the bioluminescence inhibition of bioluminescence in *A. fischeri* after 30 min of exposure to varying concentrations of the pure IL and its mixture with lithium 0.5 m. This concentration was selected due to its melting point being slightly lower

than that of the other concentrations. Despite a 50% reduction in conductivity at 298 K compared to the pure IL, it still maintains a high conductivity value.
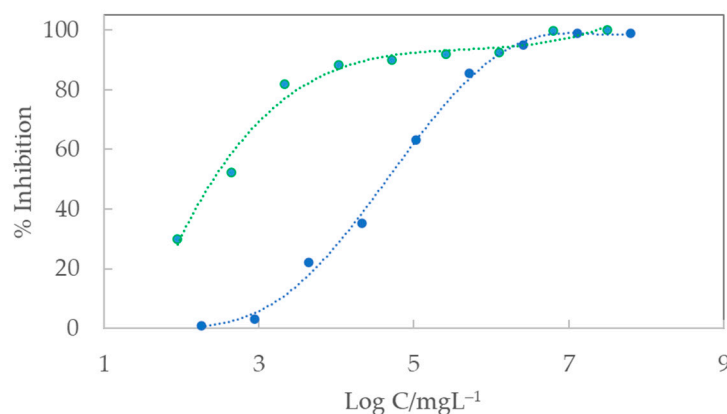

Figure 6. Inhibition of bioluminescence for 30 min of exposure against the logarithm of the concentration of (•) $[C_3C_1Pyrr][TFSI]$ and (•) $[C_3C_1Pyrr][TFSI] + [Li][TFSI]$ 0.5 m.

The inhibition responses for the analysed samples were fitted to a logistic equation. EC_{50}, EC_{20}, and EC_{10} values after 5, 15, and 30 minutes of exposure are calculated from these fitting equations and presented in Tables 6 and 7. As noted earlier, EC_{10} and EC_{20} provide initial benchmarks on the estimation of the lowest observed effect concentration, with EC_{10} being a particularly useful for assessing minimal environmental risks independently of concentration. Bacterial bioluminescence serves as a key indicator of cellular metabolism, where a decrease in luminescence reflects reduced cellular respiration [40,41]. Remarkably, the observed trend in toxic effects remains consistent across the different exposure times, suggesting a uniform mechanism of action on bacteria throughout the entire exposure period.

Table 6. Effective concentration values in mg/L for $[C_3C_1Pyrr][TFSI]$ and the corresponding 95% confidence intervals, determined after of the three selected exposure times to the marine bacteria *A. fischeri*.

[C₃C₁Pyrr][TFSI]			
Exposure Time/min	EC_{50}/mg L^{-1}	EC_{20}/mg L^{-1}	EC_{10}/mg L^{-1}
5	925.88 (741.93; 1109.83)	400.03 (258.09; 541.96)	244.70 (123.27; 366.13)
15	629.53 (423.12; 835.94)	291.98 (123.92; 460.04)	186.18 (39.69; 332.68)
30	516.32 (299.31; 733.32)	246.77 (63.47; 430.07)	160.13 (15.24; 312.40)

Table 7. Effective concentration values in mg/L for $[C_3C_1Pyrr][TFSI] + [Li][TFSI]$ 0.5 m and the corresponding 95% confidence intervals, determined after of the three selected exposure times of the marine bacteria *A. fischeri*.

[C₃C₁Pyrr][TFSI] + [Li][TFSI] 0.5 m			
Exposure Time/min	EC_{50}/mg L^{-1}	EC_{20}/mg L^{-1}	EC_{10}/mg L^{-1}
5	178.72 (152.97; 204.48)	79.19 (59.39; 98.98)	49.16 (32.62; 65.70)
15	129.34 (107.09; 151.59)	56.92 (39.86; 73.97)	35.19 (21.04; 49.33)
30	109.88 (85.34; 134.42)	47.19 (28.78; 65.61)	28.77 (13.75; 43.79)

Although no literature results were found for this compound or its mixture with lithium for *A. fischeri*, the EC_{50} values at 30 min are slightly lower than $[C_4C_1Pyrr][TFSI]$. This observation correlates well with the trend that the longer the alkyl chain, the higher the toxicity [24,41–43].

As highlighted in a previous study of our research group [23], the EC values decrease approximately 4 times after the addition of [Li][TFSI] for all exposure times. This effect was also observed for [C$_4$C$_1$Pyrr][TFSI] and [C$_4$C$_1$C$_1$Im][TFSI] [23]. Even though the toxicity of the salt itself is lower than that of the pure IL [43], this reduction can be attributed to the increased concentration of [TFSI]$^-$ anions resulting from the salt addition. The highest [TFSI]$^-$ concentration enhances the hydrophobicity of the sample, which is directly related to the bioluminescence inhibition in A. Fischeri. Despite this, according to the classification by Passino and Smith [24], both compounds can be classified within the same toxicity level: practically harmless.

4. Conclusions

In this work, the thermal and electric properties of pure [C$_3$C$_1$Pyrr][TFSI] IL and its binary mixtures with [Li][TFSI] at four different concentrations were studied, as well as the toxicity of these compounds, which was also analysed in the study. The main conclusions of the work are as follows:

- The increase in concentration of [Li][TFSI] makes the crystallization of the samples more challenging, particularly at highest scanning rate. This results in increased amorphous behaviour of the mixtures, evident from the broadening of the peaks and the appearance of the glass transition that takes place at higher temperatures when salt concentration is increased. Despite this, peaks related to crystalline behaviour (freezing and melting) remains observable for all the salt concentrations.
- The ionic conductivity of [C$_3$C$_1$Pyrr][TFSI] + [Li][TFSI] mixtures, whose behaviour against temperature is well described by the Vogel-Fulcher-Tammann (VFT) equation, decreases with [Li][TFSI] concentration. A linear increase in activation energies with salt concentration was found when fitting to Arrhenius equation, indicating that ion conduction in the electrolyte requires more energy to take place.
- The addition of salt significantly increases the toxicity of the mixture, as indicated by EC$_{50}$ values. However, this increase does not change the toxicity classification according to the criteria used in this study.

Data Availability Statement: The original contributions presented in the study are included in the article; further inquiries can be directed to the corresponding author.

Conflicts of Interest: The authors declare no conflicts of interest.

References

1. Chen, Y.; Kang, Y.; Zhao, Y.; Wang, L.; Liu, J.; Li, Y.; Liang, Z.; He, X.; Li, X.; Tavajohi, N.; et al. A Review of Lithium-Ion Battery Safety Concerns: The Issues, Strategies, and Testing Standards. *J. Energy Chem.* **2021**, *59*, 83–99. [CrossRef]
2. Xu, K. Nonaqueous Liquid Electrolytes for Lithium-Based Rechargeable Batteries. *Chem. Rev.* **2004**, *104*, 4303–4417. [CrossRef] [PubMed]
3. Lee, J.; Jeon, A.R.; Lee, H.J.; Shin, U.; Yoo, Y.; Lim, H.D.; Han, C.; Lee, H.; Kim, Y.J.; Baek, J.; et al. Molecularly Engineered Linear Organic Carbonates as Practically Viable Nonflammable Electrolytes for Safe Li-Ion Batteries. *Energy Environ. Sci.* **2023**, *16*, 2924–2933. [CrossRef]

4. Meng, T.; Young, K.H.; Wong, D.F.; Nei, J. Ionic Liquid-Based Non-Aqueous Electrolytes for Nickel/Metal Hydride Batteries. *Batteries* **2017**, *3*, 4. [CrossRef]

5. Balducci, A. Ionic Liquids in Lithium-Ion Batteries. *Top. Curr. Chem.* **2017**, *375*, 20. [CrossRef] [PubMed]

6. Parajó, J.J.; Villanueva, M.; Salgado, J. 1.Thermal Stability of Ionic Liquids. In *Synthesis, Properties, Technologies and Applications*; Fehrmann, R., Santini, C., Eds.; De Gruyter: Berlín, Germany, 2019; pp. 1–16, ISBN 9783110583632.

7. Parajó, J.J.; Otero-Mato, J.M.; Lobo Ferreira, A.I.M.C.; Varela, L.M.; Santos, L.M.N.B.F. Enthalpy of Solvation of Alkali Metal Salts in a Protic Ionic Liquid: Effect of Cation Charge and Size. *J. Mol. Liq.* **2022**, *360*, 119228. [CrossRef]

8. Kim, H.T.; Kang, J.; Mun, J.; Oh, S.M.; Yim, T.; Kim, Y.G. Pyrrolinium-Based Ionic Liquid as a Flame Retardant for Binary Electrolytes of Lithium Ion Batteries. *ACS Sustain. Chem. Eng.* **2016**, *4*, 497–505. [CrossRef]

9. Dupré, N.; Moreau, P.; De Vito, E.; Quazuguel, L.; Boniface, M.; Kren, H.; Bayle-Guillemaud, P.; Guyomard, D. Carbonate and Ionic Liquid Mixes as Electrolytes to Modify Interphases and Improve Cell Safety in Silicon-Based Li-Ion Batteries. *Chem. Mater.* **2017**, *29*, 8132–8146. [CrossRef]

10. Salvador, M.A.; Maji, R.; Rossella, F.; Degoli, E.; Ruini, A.; Magri, R. Structural and Dynamic Characterization of Li–Ionic Liquid Electrolyte Solutions for Application in Li-Ion Batteries: A Molecular Dynamics Approach. *Batteries* **2023**, *9*, 234. [CrossRef]

11. Kerner, M.; Johansson, P. Pyrrolidinium Fsi and TFSI-Based Polymerized Ionic Liquids as Electrolytes for High-Temperature Lithium-Ion Batteries. *Batteries* **2018**, *4*, 10. [CrossRef]

12. McGrath, L.M.; Rohan, J.F. Pyrrolidinium Containing Ionic Liquid Electrolytes for Li-Based Batteries. *Molecules* **2020**, *25*, 6002. [CrossRef] [PubMed]

13. Ravi, M.; Kim, S.; Ran, F.; Kim, D.S.; Lee, Y.M.; Ryou, M.H. Hybrid Gel Polymer Electrolyte Based on 1-Methyl-1-Propylpyrrolidinium Bis(Trifluoromethanesulfonyl) Imide for Flexible and Shape-Variant Lithium Secondary Batteries. *J. Memb. Sci.* **2021**, *621*, 119018. [CrossRef]

14. Yang, B.; Li, C.; Zhou, J.; Liu, J.; Zhang, Q. Pyrrolidinium-Based Ionic Liquid Electrolyte with Organic Additive and LiTFSI for High-Safety Lithium-Ion Batteries. *Electrochim. Acta* **2014**, *148*, 39–45. [CrossRef]

15. Makino, T.; Kanakubo, M.; Umecky, T.; Suzuki, A.; Nishida, T.; Takano, J. Pressure–Volume–Temperature–Composition Relations for Carbon Dioxide+pyrrolidinium-Based Ionic Liquid Binary Systems. *Fluid. Phase Equilib.* **2013**, *360*, 253–259. [CrossRef]

16. Liu, Q.; Zhao, L.; Ma, L.; Chu, J.; Wang, J.; Zang, Y. Hydroxyethyl Group Effect on Properties of Bis[(Trifluoromethyl)Sulfonyl]Imide-Type Ionic Liquids. *J. Chem. Eng. Data* **2020**, *65*, 4780–4789. [CrossRef]

17. Huang, Q.; Lourenço, T.C.; Costa, L.T.; Zhang, Y.; Maginn, E.J.; Gurkan, B. Solvation Structure and Dynamics of Li+ in Ternary Ionic Liquid–Lithium Salt Electrolytes. *J. Phys. Chem. B* **2019**, *123*, 516–527. [CrossRef]

18. Villanueva, M.; Parajó, J.J.; Sánchez, P.B.; García, J.; Salgado, J. Liquid Range Temperature of Ionic Liquids as Potential Working Fluids for Absorption Heat Pumps. *J. Chem. Thermodyn.* **2015**, *91*, 127–135. [CrossRef]

19. Parajó, J.J.; Villanueva, M.; Sánchez, P.B.; Salgado, J. Liquid Window of Some Biologically-Active Ionic Liquids. *J. Chem. Thermodyn.* **2018**, *126*, 1–10. [CrossRef]

20. Salgado, J.; Parajó, J.J.; Villanueva, M.; Rodríguez, J.R.; Cabeza, O.; Varela, L.M. Liquid Range of Ionic Liquid–Metal Salt Mixtures for Electrochemical Applications. *J. Chem. Thermodyn.* **2019**, *134*, 164–174. [CrossRef]

21. Leys, J.; Wübbenhorst, M.; Preethy Menon, C.; Rajesh, R.; Thoen, J.; Glorieux, C.; Nockemann, P.; Thijs, B.; Binnemans, K.; Longuemart, S. Temperature Dependence of the Electrical Conductivity of Imidazolium Ionic Liquids. *J. Chem. Phys.* **2008**, *128*, 064509. [CrossRef]

22. Parajó, J.J.; Santiago-Alonso, A.; Vallet, P.; Teijeira, T.; Emeterio, R.S.; Villanueva, M.; Salgado, J. Comprehensive Analysis of the Acute Toxicity of Ionic Liquids Using Microtox® Bioassays. *Appl. Sci.* **2024**, *14*, 2480. [CrossRef]

23. Parajó, J.J.; Vallet, P.; Varela, L.M.; Villanueva, M.; Salgado, J. Ecotoxicity of Binary Mixtures of ILs and Inorganic Salts of Electrochemical Interest. *Environ. Sci. Pollut. Res.* **2022**, *29*, 24983–24994. [CrossRef] [PubMed]

24. Passino, D.R.M.; Smith, S.B. Acute Bioassays and Hazard Evaluation of Representative Contaminants Detected in Great Lakes Fish. *Environ. Toxicol. Chem.* **1987**, *6*, 901–907. [CrossRef]

25. Shi, B.; Wang, Z.; Wen, H. Research on the Strengths of Electrostatic and van Der Waals Interactions in Ionic Liquids. *J. Mol. Liq.* **2017**, *241*, 486–488. [CrossRef]

26. Salminen, J.; Papaiconomou, N.; Kumar, R.A.; Lee, J.-M.; Kerr, J.; Newman, J.; Prausnitz, J.M. Physicochemical Properties and Toxicities of Hydrophobic Piperidinium and Pyrrolidinium Ionic Liquids. *Fluid. Phase Equilib.* **2007**, *261*, 421–426. [CrossRef]

27. MacFarlane, D.R.; Meakin, P.; Sun, J.; Amini, N.; Forsyth, M. Pyrrolidinium Imides: A New Family of Molten Salts and Conductive Plastic Crystal Phases. *J. Phys. Chem. B* **1999**, *103*, 4164–4170. [CrossRef]

28. Huang, Q.; Lee, Y.-Y.; Gurkan, B. Pyrrolidinium Ionic Liquid Electrolyte with Bis(Trifluoromethylsulfonyl)Imide and Bis(Fluorosulfonyl)Imide Anions: Lithium Solvation and Mobility, and Performance in Lithium Metal–Lithium Iron Phosphate Batteries. *Ind. Eng. Chem. Res.* **2019**, *58*, 22587–22597. [CrossRef]

29. Henderson, W.A.; Passerini, S. Phase Behavior of Ionic Liquid−LiX Mixtures: Pyrrolidinium Cations and TFSI- Anions. *Chem. Mater.* **2004**, *16*, 2881–2885. [CrossRef]

30. Appetecchi, G.B.; Montanino, M.; Carewska, M.; Moreno, M.; Alessandrini, F.; Passerini, S. Chemical–Physical Properties of Bis(Perfluoroalkylsulfonyl)Imide-Based Ionic Liquids. *Electrochim. Acta* **2011**, *56*, 1300–1307. [CrossRef]

31. Gómez, E.; Calvar, N.; Domínguez, Á.; Macedo, E.A. Thermal Behavior and Heat Capacities of Pyrrolidinium-Based Ionic Liquids by DSC. *Fluid. Phase Equilib.* **2018**, *470*, 51–59. [CrossRef]

32. Annat, G.; Forsyth, M.; MacFarlane, D.R. Ionic Liquid Mixtures—Variations in Physical Properties and Their Origins in Molecular Structure. *J. Phys. Chem. B* **2012**, *116*, 8251–8258. [CrossRef] [PubMed]

33. González, B.; González, E.J. Physical Properties of the Pure 1-Methyl-1-Propylpyrrolidinium Bis(Trifluoromethylsulfonyl)Imide Ionic Liquid and Its Binary Mixtures with Alcohols. *J. Chem. Thermodyn.* **2014**, *68*, 109–116. [CrossRef]

34. Vallet, P.; Parajó, J.J.; Santiago-Alonso, A.; Villanueva, M.; Varela, L.M.; Salgado, J. Thermal Characterization of [C2Im][NO$_3$] and Multivalent Nitrate Salts Mixtures. *Crystals* **2024**, *14*, 502. [CrossRef]

35. Parajó, J.J.; Vallet, P.; Villanueva, M.; Cabeza, O.; Fernández-Carretero, F.; García Luis, A.; Di Pietro, M.E.; Mele, A.; Castiglione, F.; Salgado, J.; et al. Ionogels Based on Protic Ionic Liquid-Lithium Salt Mixtures. *J. Mol. Liq.* **2024**, *397*, 124093. [CrossRef]

36. Martinelli, A.; Matic, A.; Jacobsson, P.; Börjesson, L.; Fernicola, A.; Scrosati, B. Phase Behavior and Ionic Conductivity in Lithium Bis(Trifluoromethanesulfonyl)Imide-Doped Ionic Liquids of the Pyrrolidinium Cation and Bis(Trifluoromethanesulfonyl)Imide Anion. *J. Phys. Chem. B* **2009**, *113*, 11247–11251. [CrossRef]

37. Vallet, P.; Bouzón-Capelo, S.; Méndez-Morales, T.; Gómez-González, V.; Arosa, Y.; de la Fuente, R.; López-Lago, E.; Rodríguez, J.R.; Gallego, L.J.; Parajó, J.J.; et al. On the Physical Properties of Mixtures of Nitrate Salts and Protic Ionic Liquids. *J. Mol. Liq.* **2022**, *350*, 118483. [CrossRef]

38. Tsamopoulos, A.J.; Wang, Z.-G. Ion Conductivity in Salt-Doped Polymers: Combined Effects of Temperature and Salt Concentration. *ACS Macro Lett.* **2024**, *13*, 322–327. [CrossRef]

39. Petrowsky, M.; Frech, R. Salt Concentration Dependence of the Compensated Arrhenius Equation for Alcohol-Based Electrolytes. *Electrochim. Acta* **2010**, *55*, 1285–1288. [CrossRef]

40. Abbas, M.; Adil, M.; Ehtisham-ul-Haque, S.; Munir, B.; Yameen, M.; Ghaffar, A.; Shar, G.A.; Asif Tahir, M.; Iqbal, M. Vibrio Fischeri Bioluminescence Inhibition Assay for Ecotoxicity Assessment: A Review. *Sci. Total Environ.* **2018**, *626*, 1295–1309. [CrossRef]

41. Silva, F.A.; Coutinho, J.A.P.; Ventura, S.P.M. *Aquatic Toxicology of Ionic Liquids (ILs) in Encyclopedia of Ionic Liquids*, 1st ed.; Springer Nature: Berlín, Germany, 2019.

42. Villanueva, M.; Vallet, P.; Teijeira, T.; Santiago-Alonso, A.; Amigo, A.; Tojo, E.; Varela, L.M.; Parajó, J.J.; Salgado, J. Effect of Alkyl Chain Length on the Thermal Properties and Toxicity of N-Alkyl-Ammonium Nitrate Ionic Liquids (n = 2, 3, 4, 5, 6, 8) for Energy Applications. *J. Therm. Anal. Calorim.* **2024**. [CrossRef]

43. Viboud, S.; Papaiconomou, N.; Cortesi, A.; Chatel, G.; Draye, M.; Fontvieille, D. Correlating the Structure and Composition of Ionic Liquids with Their Toxicity on Vibrio Fischeri: A Systematic Study. *J. Hazard. Mater.* **2012**, *215–216*, 40–48. [CrossRef] [PubMed]